

DIRECT AND COMPOUND NUCLEUS REACTIONS FOR THE SYSTEM ${}^7\text{Be} + {}^{58}\text{Ni}$ AT NEAR-BARRIER ENERGIES*

M. MAZZOCCO^{a,b}, D. TORRESI^{a,b}, L. ACOSTA^c, A. BOIANO^d
 C. BOIANO^e, N. FIERRO^a, T. GLODARIU^f, A. GUGLIELMETTI^{e,g}
 N. KEELEY^h, M. LA COMMARA^{d,i}, I. MARTEL^c, C. MAZZOCCHI^j
 P. MOLINI^{a,b}, A. PAKOU^k, C. PARASCANDOLO^{a,b}, V.V. PARKAR^c
 N. PATRONIS^k, D. PIERROUTSAKOU^d, M. ROMOLI^d, K. RUSEK^l
 A.M. SANCHEZ-BENITEZ^c, M. SANDOLI^{d,i}, C. SIGNORINI^{a,b}
 R. SILVESTRI^{d,i}, F. SORAMEL^{a,b}, E. STILIARIS^m, E. STRANO^{a,b}
 L. STROE^f, K. ZERVA^k

^aDipartimento di Fisica e Astronomia, Università di Padova, Padova, Italy

^bINFN — Sezione di Padova, Padova, Italy

^cDepartamento de Física Aplicada, Universidad de Huelva, Huelva, Spain

^dINFN — Sezione di Napoli, Napoli, Italy

^eINFN — Sezione di Milano, Milano, Italy

^fNIPNE, Magurele, Romania

^gUniversità degli Studi di Milano, Milano, Italy

^hDepartment of Nuclear Reactions, INS, Warszawa, Poland

ⁱDipartimento di Scienze Fisiche, Università di Napoli, Napoli, Italy

^jFaculty of Physics, University of Warsaw, Warszawa, Poland

^kDepartment of Physics and HINP, University of Ioannina, Ioannina, Greece

^lHeavy Ion Laboratory, University of Warsaw, Warszawa, Poland

^mDepartment of Physics, University of Athens, Athens, Greece

(Received December 10, 2013)

The interaction of the Radioactive Ion Beam ${}^7\text{Be}$ with the closed proton shell target ${}^{58}\text{Ni}$ was investigated at two energies around the Coulomb barrier. ${}^7\text{Be}$ scattered ions as well as ${}^{3,4}\text{He}$ reaction products were measured in a rather wide angular range. The elastic scattering angular distributions were analyzed within the framework of the optical model to extract the total reaction cross section. Extensive theoretical and kinematical calculations were performed to disentangle the origin of ${}^{3,4}\text{He}$ ions between direct and compound nucleus reactions.

DOI:10.5506/APhysPolB.45.363

PACS numbers: 25.60.Bx, 25.60.Dz

* Presented at the XXXIII Mazurian Lakes Conference on Physics, Piaski, Poland, September 1–7, 2013.

1. Introduction

Light nuclei, even in the vicinity of the β -stability valley, may exhibit very exotic features and provide very powerful benchmarks for modern theoretical nuclear models. Some of these nuclei, such as for instance ${}^6\text{He}$, ${}^{11}\text{Be}$ and ${}^{11}\text{Li}$, have very peculiar shapes, which can be described by a (mostly) inert core surrounded by a halo of rarefied nuclear matter. Some other light nuclei, such as ${}^8\text{He}$, ${}^{14}\text{Be}$ or ${}^{22}\text{C}$, are characterized by neutron skin structures, *i.e.* rather “thick” neutron skins close to the nuclear surface. In addition, most of these nuclei have very low particle emission thresholds (S_p , S_n or $S_\alpha < 1.0$ MeV) and may present very well pronounced cluster structures.

All these peculiar properties may strongly influence the reaction dynamics, especially at energies around the Coulomb barrier. Several review papers have been recently published on this topic [1–4]. In earlier measurements, large attention was paid to the effects of the nuclear halo on the fusion probability. Over the last decade, the focus has shifted towards the investigation of the role played by direct reaction channels, since they turned out to be strongly enhanced by the projectile exotic features.

Among all light ions, we selected the radioactive and weakly-bound ${}^7\text{Be}$ as subject of our investigation. ${}^7\text{Be}$ has a quite low particle emission threshold ($S_\alpha = 1.586$ MeV) and a very well pronounced ${}^3\text{He}$ – ${}^4\text{He}$ cluster structure. Thus, while approaching a target nucleus, ${}^7\text{Be}$ has a large probability either to breakup into its constituent clusters or to transfer one of them to the target. The fact that the two ${}^7\text{Be}$ clusters, *i.e.* ${}^3\text{He}$ and ${}^4\text{He}$, are stable, well-bound, and have similar masses greatly simplifies life to experimentalists, since the same technique can be adopted for the simultaneous and unambiguous detection of both of them. The set-up would be much more complex in the case of detailed reaction dynamics studies involving projectiles breaking up into the pair neutron(s)+core, *e.g.* ${}^{6,8}\text{He}$, ${}^{11}\text{Li}$, ${}^{11}\text{Be}$, or when the projectile may break into clusters with completely different masses, and, in turn, energies, as it is the case for the weakly-bound ${}^{17}\text{F}$ breaking up into ${}^{16}\text{O}+p$.

So far, the ${}^7\text{Be}$ -induced reaction dynamics at Coulomb barrier energies has been investigated for the systems ${}^7\text{Be}+{}^{238}\text{U}$ [5] and ${}^7\text{Be}+{}^{58}\text{Ni}$ [6]. In the former reaction, the fusion–fission and transfer/breakup–fission cross sections were measured at five different bombarding energies. In the latter system, the scattering process was measured and the total reaction cross section extracted for five beam energies. Our experiment was able for the first time to unambiguously detect (and distinguish) ${}^3\text{He}$ and ${}^4\text{He}$ reaction products for the system ${}^7\text{Be}+{}^{58}\text{Ni}$, providing new insights on the ${}^7\text{Be}$ -induced reaction dynamics at near-barrier energies.

The paper is organized as follows: in Sec. 2, the ${}^7\text{Be}$ Radioactive Ion Beam (RIB) production technique and the experimental set-up will be described. The results of the elastic scattering measurement and the experimental ${}^3\text{He}$ and ${}^4\text{He}$ angular distributions will be discussed in Sec. 3 and Sec. 4, respectively. Detailed theoretical and kinematical calculations for different direct processes and the interplay between direct and compound nucleus reactions will be covered in Sec. 5. Some concluding remarks will finally be given in Sec. 6.

2. Experiment

2.1. ${}^7\text{Be}$ beam production

The experiment was performed at the Laboratori Nazionali di Legnaro (LNL) of the Istituto Nazionale di Fisica Nucleare (INFN) in Italy. The ${}^7\text{Be}$ RIB was produced with the in-flight technique by means of the facility EXOTIC [7]. The facility was commissioned in 2004 and now is fully operational for the production of light weakly-bound RIBs.

A ${}^7\text{Li}$ primary beam delivered by the LNL XTU tandem accelerator at 34.2 MeV beam energy and with an intensity of about 100 pA was impinging on a H_2 gas target. The gas was contained in 5-cm long cell, doubly-walled with 2.2- μm thick havar foils. The target station was operated at 1 bar and cooled down to liquid nitrogen temperature, ensuring an overall target thickness of about 1.35 mg/cm². The ${}^7\text{Be}$ production reaction was $p({}^7\text{Li}, {}^7\text{Be})n$ with $Q_{\text{val}} = -1.64$ MeV. The RIB under production was selected by means of a 30°-bending magnet and a 1-m long Wien filter. The outgoing ${}^7\text{Be}$ beam has an energy of 22.3 ± 0.4 MeV, an intensity of $2\text{--}3 \times 10^5$ pps and nearly 100-% purity. An additional ${}^7\text{Be}$ beam energy was obtained by inserting a 10- μm thick aluminium degrader in a proper location along the beam line. The second ${}^7\text{Be}$ energy resulted to be 17.7 ± 0.5 MeV. These energy values corresponded to approximately +10% and -10% of the nominal Coulomb barrier for the reaction on a 1-mg/cm² thick ${}^{58}\text{Ni}$ target. The total acquisition times were about 3 and 1.5 days at the higher and lower secondary beam energy, respectively.

2.2. The detector array DINEX

Charged reaction products were detected by means of the detector array DINEX [8]. It consisted of 8 Double Sided Silicon Strip Detectors (DSSSDs) arranged in 4 ΔE (42–48 μm)– E (1000 μm) telescopes. Each detector had an active area of 48×48 mm² and each side was segmented into 16 strips, ensuring a pixel resolution of 3×3 mm². The thickness of the ΔE layers allowed the unambiguous identification of ${}^3\text{He}$ and ${}^4\text{He}$ ions whose kinetic energies were larger than 6.5 and 7.2 MeV, respectively. The telescopes were

located at an average distance of 71 mm from the ^{58}Ni target, providing an overall solid angle coverage of about 10% of 4π sr. The mean polar angles of the four telescopes were the following: $+57^\circ$ (T1), $+128^\circ$ (T2), -61.5° (T3), -132° (T4). Angles were considered positive (negative) for detectors located in the left (right) hemisphere from a downstream view of the scattering chamber.

3. Quasi-elastic scattering and total reaction cross section

Figure 1 shows the total energy spectrum collected by a vertical strip of the ΔE layer of telescope T1 for the reaction at 22.3 MeV beam energy. The thin/black histogram represents the experimental data, while the thick/red solid line is the results of a Monte Carlo simulation for a pure elastic scattering process. The simulation took into account: (i) the energy and position

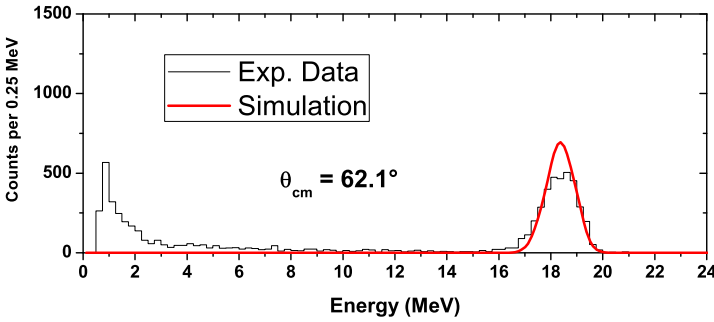


Fig. 1. Total energy spectrum collected by a vertical strips of telescope T1 located at $\theta_{cm} = 62.1^\circ$ for the reaction ${}^7\text{Be}+{}^{58}\text{Ni}$ at 22.3 MeV beam energy. The black histogram represents the experimental data, while solid (red) line is the results of a Monte Carlo simulation for a pure elastic scattering process. See the text for additional details.

resolution of the secondary beam; (ii) the ${}^7\text{Be}$ energy loss inside the ${}^{58}\text{Ni}$ target prior and after the scattering process; (iii) the kinematics of the elastic scattering process; (iv) the geometrical arrangement of the detector set-up. Finally, a pure Rutherford cross section over the entire angular range was assumed for the simulated data. Therefore, the strip-by-strip ratio between the integrals of the experimental and simulated elastic scattering peaks immediately gave the ratio-to-Rutherford ($d\sigma/d\sigma_{\text{Ruth}}$) for the corresponding strip. Simulated spectra were normalized at very forward angles ($\theta_{cm} < 60^\circ$), where the elastic scattering differential cross section was described by the well-known Rutherford formula. A 3.5-% systematic error was estimated for the overall normalization procedure. Figure 2 shows the elastic scattering angular distributions we evaluated for the reaction ${}^7\text{Be}+{}^{58}\text{Ni}$ at 22.3 MeV.

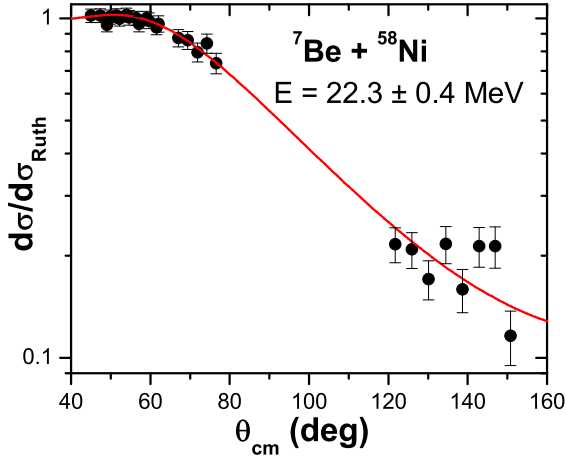


Fig. 2. Quasi-elastic angular distribution for the reaction ${}^7\text{Be} + {}^{58}\text{Ni}$ at 22.3 MeV beam energy. Plotted errors include the statistical uncertainty and a 3.5-% systematic error, related to normalization procedure of the data (additional details are given in the text). The solid (red) line is the result of an optical model best-fit analysis of the collected data.

Since the ${}^7\text{Be}$ secondary beam energy resolution and the ${}^{58}\text{Ni}$ target thickness did not allow us to clearly distinguish between pure elastic scattering events and inelastic excitations leading to ${}^7\text{Be}$ and ${}^{58}\text{Ni}$ first excited states at 0.429 MeV and 1.414 MeV, respectively, data plotted in Fig. 2 have to be considered as “quasi”-elastic.

The experimental angular distribution shown in Fig. 2 was fitted within the framework of the optical model with the subroutine SFresco of the main code Fresco [9], in order to extract the total reaction cross section. The outcoming theoretical curve is displayed with a solid (red) line in Fig. 2. A total reaction cross section of 561 mb was obtained from the present analysis. This value is in fairly good agreement with the data trend individuated by the measurements at lower beam energies [6]. Finally, the quasi-elastic scattering data collected at 17.7 MeV beam energy (already measured by Aguilera and collaborators [6]), were substantially used to provide an additional consistency cross-check of the data normalization procedure at forward angles. The statistics collected at backward angles was enough to evaluate only an overall ratio-to-Rutherford estimate, whereas it was not sufficient to derive a proper quasi-elastic angular distribution.

4. ${}^3\text{He}$ and ${}^4\text{He}$ angular distributions

ΔE - E correlation plots at 22.3 MeV beam energy showed both at forward and backward angles quite large ${}^3\text{He}$ and ${}^4\text{He}$ production yields. Several reaction mechanisms can account for the presence of ${}^3\text{He}$ and ${}^4\text{He}$ ions in the reaction exit channel. Nevertheless, the only process producing at the same time a ${}^3\text{He}$ - ${}^4\text{He}$ pair is the exclusive breakup channel ${}^7\text{Be} \rightarrow {}^3\text{He} + {}^4\text{He}$. Being the ${}^4\text{He}$ production yield a factor of (at least) 4 larger than that for ${}^3\text{He}$, we could immediately deduce that, in this energy range, the exclusive breakup channel plays a minor role in the reaction dynamics for the system ${}^7\text{Be} + {}^{58}\text{Ni}$. Possible contributions from the incomplete fusion process are presently under evaluation with the semi-classical code PLATYPUS [10]. In the meanwhile, we devoted our attention to other reaction channels, namely transfer channels and the fusion-evaporation process.

4.1. ${}^3\text{He}$ production

We started our investigation from ${}^3\text{He}$, since there are fewer processes leading to presence of ${}^3\text{He}$ in the reaction output channel. We considered the following mechanisms:

- ${}^4\text{He}$ -stripping: ${}^7\text{Be} + {}^{58}\text{Ni} \rightarrow {}^3\text{He} + {}^{61}\text{Zn}$ ($Q_{gg} = +1.78$ MeV);
- exclusive breakup: ${}^7\text{Be} \rightarrow {}^4\text{He} + {}^3\text{He}$ ($S_\alpha = 1.586$ MeV).

Figure 3 shows the ${}^3\text{He}$ energy spectrum (black (thin) histogram) measured by telescope T1. The solid lines are the results of Monte Carlo simulations performed using a package similar to that employed for the elastic scattering process and, of course, including the kinematics of the reaction mechanism under consideration. For the ${}^4\text{He}$ -stripping process, we followed the semi-classical model of Brink [11] by considering in the simulation the population of excited states of the target-like particle at excitation energies in an interval of 4 MeV around the central value of $E_x = 10.81$ MeV. For the breakup process, we considered a projectile excitation energy of $E_x = 3.0 \pm 0.5$ MeV above the breakup threshold. This energy value was chosen since it corresponds to a well-known ${}^7\text{Be}$ resonance. In this explorative phase, constant angular distributions in the center-of-mass frame were assumed for the ejectiles. In this way, we can have a first idea concerning the energy intervals foreseen for the different processes. More detailed simulations will be carried out in the near future by using the results of precise theoretical calculations for the two processes. Finally, the calculated energy spectra were properly normalized so that their integral above the ${}^3\text{He}$ ΔE punching through energy (about 6 MeV in the case of telescope T1) were

equal to the number of ${}^3\text{He}$ ions experimentally detected. We can clearly see from Fig. 3 that the ${}^3\text{He}$ experimental energy spectrum is rather compatible with that predicted for a ${}^4\text{He}$ -stripping process.

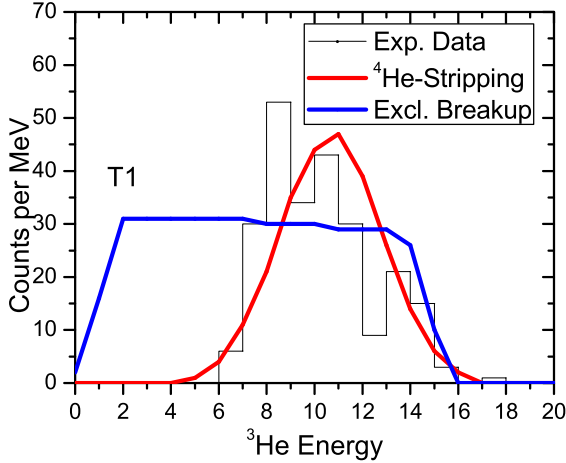


Fig. 3. ${}^3\text{He}$ energy spectrum collected for the reaction ${}^7\text{Be} + {}^{58}\text{Ni}$ at 22.3 MeV beam energy by the telescope T1. The black (thin) histogram represents the experimental data, while the solid lines are the results of Monte Carlo calculations for the ${}^4\text{He}$ -stripping process (gray/red) and the exclusive breakup channel (light gray/blue). See the text for additional details.

4.2. ${}^4\text{He}$ production

The number of nuclear processes leading to the presence of ${}^4\text{He}$ in the reaction output channel is sensibly larger than for ${}^3\text{He}$. In our analysis we considered:

- ${}^3\text{He}$ -stripping: ${}^7\text{Be} + {}^{58}\text{Ni} \rightarrow {}^4\text{He} + {}^{62}\text{Zn}$ ($Q_{gg} = +9,46$ MeV);
- exclusive breakup: ${}^7\text{Be} \rightarrow {}^4\text{He} + {}^3\text{He}$ ($S_{\alpha} = 1.586$ MeV);
- n -stripping: ${}^7\text{Be} + {}^{58}\text{Ni} \rightarrow {}^6\text{Be}(= {}^4\text{He} + 2p) + {}^{59}\text{Ni}$ ($Q_{gg} = 1.68$ MeV);
- n -pickup: ${}^7\text{Be} + {}^{58}\text{Ni} \rightarrow {}^8\text{Be}(= 2{}^4\text{He}) + {}^{57}\text{Ni}$ ($Q_{gg} = +6.68$ MeV);
- ${}^4\text{He}$ evaporation after compound nucleus formation (complete fusion).

Figure 4 displays the ${}^4\text{He}$ experimental energy distribution at forward angles together with the energy spectra calculated with a Monte Carlo simulation, following a procedure similar to those already described for the elastic scattering process and for the ${}^3\text{He}$ production. In this case, for the

^3He -stripping we assumed the population of target-like fragment excited states at energies around $E_x = 18.49$ MeV, for the n -stripping channel only the ground state to ground state transition was considered, while for the n -pickup process the population of excited states of the target-like fragment with excitation energies around $E_x = Q_{gg}$ were taken into account. Finally, the statistical model PACE2 [12] was employed for the calculation of the energy spectra for alpha particles emitted after a fusion–evaporation reaction.

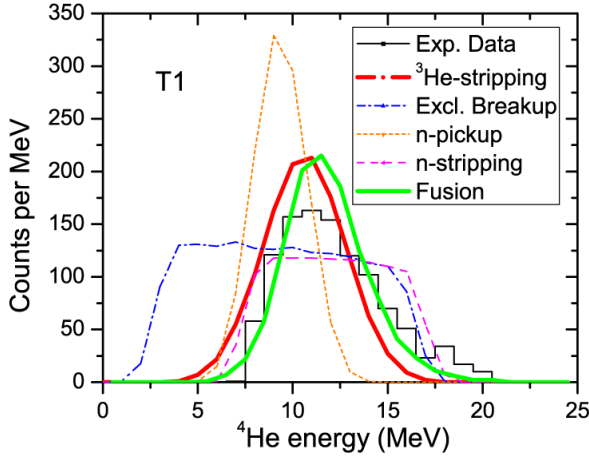


Fig. 4. ^4He energy spectrum collected for the reaction $^7\text{Be} + ^{58}\text{Ni}$ at 22.3 MeV beam energy by telescope T1. The black (thin) histogram represents the experimental data, while the lines are the results of Monte-Carlo calculations for the ^3He -stripping process (solid black/red), the exclusive breakup channel (dot-dashed blue), the n -pickup (dotted orange), the n -stripping (dashed pink) and fusion–evaporation (gray/green).

The comparison between the ^4He experimental energy spectra and those simulated shows that the origin of ^4He particles is mainly compatible with a ^3He -stripping transfer or with the fusion process. The tiny shift between the simulated ^4He energy distributions for these two processes is too small to be unambiguously disentangled by the statistics collected during our experiment.

In addition, we notice that fusion–evaporation and ^3He -stripping are the only processes leading to the presence of only one ^4He particle in the reaction output channel. The other considered processes would give rise to a ^3He – ^4He pair (exclusive breakup), to a ^4He – p coincidence event (n -stripping, after the ^6Be breakup into $^4\text{He}+2p$) or to a ^4He – ^4He coincidence event (n -pickup, after the ^8Be breakup into two ^4He). Therefore, the analysis of coincidence events (as recently done for the reactions $^6,7\text{Li}+^{207,208}\text{Pb}$,

${}^{209}\text{Bi}$ [13]) would give us an additional clue in figuring out the origin of ${}^3\text{He}$ and ${}^4\text{He}$ particles. Within the statistical accuracy of our experiment and the solid angle coverage of our detector set-up, we did not detect any coincidences between ${}^1\text{H}$ - ${}^4\text{He}$, ${}^3\text{He}$ - ${}^4\text{He}$ and ${}^4\text{He}$ - ${}^4\text{He}$ pairs. We thus could only quote the cross section upper limits for these three processes. Our preliminary evaluations are the following: $\sigma < 3$ mb for the exclusive breakup process, $\sigma < 7$ mb for the n -stripping channel and $\sigma < 6$ mb for the n -pick transfer.

At the same time we performed theoretical calculations within the Continuum Discretized Coupled Channel (CDCC) approach for the exclusive breakup process and within the Distorted Wave Born Approximation (DWBA) formalism for the n -stripping and n -pickup transfer channels. Figure 5 shows the results of our calculations and directly compares them to the ${}^3\text{He}$ and ${}^4\text{He}$ angular distribution data. We clearly see that the theoretical curves underestimate by far the experimental values. The angle-integrated cross sections for these three processes are 9.3 mb, 10.3 mb and 5.8 mb for the exclusive breakup, the n -stripping and the n -pick processes, respectively. The calculated values are in rather good agreement, within the statistical accuracy of our experiment, with the upper limits we obtained from the evaluation of the “missing” coincidences between ${}^1\text{H}$, ${}^3\text{He}$ and ${}^4\text{He}$ ions.

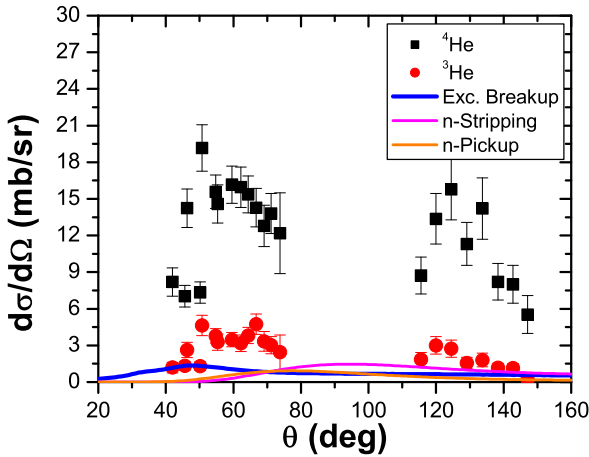


Fig. 5. Comparison between the experimental ${}^3\text{He}$ (gray/red dots) and ${}^4\text{He}$ (black squares) angular distributions and the theoretical predictions for the exclusive breakup (black/blue line), n -stripping (dark gray/pink line) and n -pickup (light gray/orange line).

5. Discussion

At the present stage of the analysis, we came to the conclusion that ${}^3\text{He}$ ions are mainly originated by the ${}^4\text{He}$ -stripping process, while ${}^4\text{He}$ particles

could essentially arise from the ^3He -stripping and the fusion–evaporation channels. On the other side, exclusive breakup, n -stripping and n -pickup are expected to play a rather minor role. Can we now put some steps forward towards disentangling the origin of ^4He ions?

We used the code PACE2 to evaluate the expected angular distribution and the multiplicity of alpha particles in the reaction $^7\text{Be}+^{58}\text{Ni}$ at 22.3 MeV beam energy. The theoretical curve was normalized to average of the ^4He experimental differential cross section in the range $\theta_{\text{lab}} = [40^\circ, 50^\circ]$. The angle-integrated cross section of the evaporated alpha particle turned out to be 80 ± 10 mb, which, taking into account a preliminary evaluation of 0.35 for the alpha multiplicity, gave an overall fusion cross section of 229 ± 29 mb. This value corresponds to $41 \pm 5\%$ of the total reaction cross section extracted from the measurement of the quasi-elastic scattering process. However, even after a point-by-point subtraction of the statistical model contribution, the theoretical curves for exclusive breakup, n -stripping and n -pickup processes still largely underpredicted the experimental ^4He angular distribution.

We thus assumed that, based on our analysis, the ^4He angular distribution remaining after the subtraction of the all reaction channels already theoretically accounted for should be attributed to the ^3He -stripping. A similar argument was employed for the ^3He angular distribution. In the latter case, the contribution of the ^4He -stripping was evaluated by subtracting only the exclusive breakup angular distribution from the experimental ^3He differential cross section. We are perfectly aware that this is a quite daring operation, especially because we do not know the behavior of the $^3,4\text{He}$ angular distributions in the interval $\Theta_{\text{lab}} = [75^\circ, 115^\circ]$. Preliminary estimates, based on a simple linear interpolation between the $^3,4\text{He}$ angular distributions measured by telescopes T1 and T3 at forward angles and by telescope T4 at backward angles, gave cross section lowest limits for the ^3He -stripping and ^4He -stripping of 54.1 mb and 18.2 mb, respectively. Adding up all cross sections evaluated so far, *i.e.* (i) inelastic excitations and exclusive breakup computed with the CDCC formalism, (ii) n -stripping and n -pick calculated with the DWBA approach, (iii) fusion obtained with the code PACE2 and, finally, (iv) the obtained lowest limits for the ^3He - and ^4He -stripping, we exhausted about 3/4 of the total reaction cross section extracted for the optical model analysis of the quasi-elastic angular distribution. We thus still have about 150 mb of the total reaction cross section unaccounted for. Do we have any chances to formulate a hypothesis about the reaction channel(s) mainly responsible for the missing contribution to the total reaction cross section?

A possible answer to this question may be given after a close inspection of the data published by Raabe and collaborators for the system $^7\text{Be}+^{238}\text{U}$ [5]. In their experiment, both fusion and direct processes were ultimately

producing a fission event, but they could clearly distinguished between each other, since in case of direct processes an additional projectile fragment would have been detected in coincidence with the two fission fragments. Direct processes clearly dominate the reaction cross section at sub-barrier energies, while compound nucleus reactions are more relevant in the above-barrier regime. In our experiment, we computed for the system ${}^7\text{Be} + {}^{58}\text{Ni}$, a fusion cross section of 229 ± 29 mb, corresponding to $41 \pm 5\%$ of the total reaction cross section. At the same downscaled beam energy (to account for the different Coulomb barrier heights), the fusion cross section for the system ${}^7\text{Be} + {}^{238}\text{U}$ exhausts about 44% of the total reaction cross section. If the similarity between the two systems may be exploited, we may conclude that the about 150 mb “missing” contribution to the total reaction cross section for the reaction ${}^7\text{Be} + {}^{58}\text{Ni}$ might arise from direct processes, namely ${}^3\text{He}$ - and ${}^4\text{He}$ -stripping.

6. Concluding remarks

The interaction of the ${}^7\text{Be}$ RIB with the closed proton shell ${}^{58}\text{Ni}$ target was investigated at two energies around the Coulomb barrier. The ${}^7\text{Be}$ radioactive beam was produced with the facility EXOTIC at INFN-LNL, which is now fully operational for the production of light weakly-bound RIBs. The analysis of the quasi-elastic differential cross section allowed the extraction of the total reaction cross section, which is in rather good agreement with the data trend individuated by earlier measurements at lower energies performed by Aguilera and collaborators [6]. Fairly large ${}^3\text{He}$ and ${}^4\text{He}$ production yields were observed at the higher beam energy and for the first time we were able to unambiguously distinguish the two helium isotopes in a ${}^7\text{Be}$ -induced experiment. ${}^4\text{He}$ ions were found to be at least 4 times more abundant than the lighter counterparts. This outcome already ruled out that possibility that the breakup channel ${}^7\text{Be} \rightarrow {}^4\text{He} + {}^3\text{He}$ would be the dominant reaction mechanism in this energy range. Detailed theoretical and kinematical calculations together with the exploited similarity with the system ${}^7\text{Be} + {}^{238}\text{U}$ suggest that ${}^3\text{He}$ and ${}^4\text{He}$ are mainly originated by direct transfer channels with large positive Q -values: the ${}^4\text{He}$ - and the ${}^3\text{He}$ -stripping process, respectively. To corroborate this outcome, in a future experiment, one would need to measure the ${}^{3,4}\text{He}$ angular distribution in the angular range not covered by our experiment. On the other side, transfer channels leading to very high excitation energy states in the target-like particle, as it is the case in the present experiment for both ${}^3\text{He}$ - and ${}^4\text{He}$ -stripping, should be properly included in the theoretical calculations. Unfortunately, this task is still at the limits of present day theoretical models for the reaction dynamics at Coulomb barrier energies.

REFERENCES

- [1] L.F. Canto *et al.*, *Phys. Rep.* **424**, 1 (2006).
- [2] N. Keeley *et al.*, *Prog. Part. Nucl. Phys.* **59**, 579 (2007).
- [3] M. Mazzocco, *Int. J. Mod. Phys.* **E19**, 977 (2010).
- [4] M. Mazzocco *et al.*, *Acta Phys. Pol. B* **44**, 437 (2013).
- [5] R. Raabe *et al.*, *Phys. Rev.* **C74**, 044606 (2006).
- [6] E.F. Aguilera *et al.*, *Phys. Rev.* **C79**, 021601 (2009).
- [7] F. Farinon *et al.*, *Nucl. Instrum. Methods* **B266**, 4097 (2008).
- [8] A.M. Sanchez-Benitez *et al.*, *J. Phys. G* **31**, S1953 (2005).
- [9] I.J. Thompson, *Comput. Phys. Rep.* **7**, 167 (1988).
- [10] A. Diaz-Torres, *Comput. Phys. Commun.* **182**, 1100 (2011).
- [11] D.M. Brink, *Phys. Lett.* **B40**, 37 (1972).
- [12] A. Gavron, *Phys. Rev.* **C21**, 230 (1980).
- [13] D.H. Luong *et al.*, *Phys. Rev.* **C88**, 034609 (2013).